




# High-Spatial Resolution Mascon Solution Over High Mountain Asia Constrained by Multisource Prior Information

Wei Wang, Yunzhong Shen , Qiuji Chen , and Fengwei Wang 

**Abstract**—High mountain Asia (HMA) holds the largest concentration of glaciers outside the polar regions, and the melting glaciers provide freshwater for more than one billion people. Therefore, it is crucial to estimate glacier mass changes over HMA. Though Gravity Recovery and Climate Experiment (GRACE) and GRACE Follow-On (GRACE-FO) can accurately monitor monthly global mass changes, the low spatial resolution of  $\sim 300$  km limits the ability to reveal detailed spatiotemporal characteristics of mountain glacier changes. In this contribution, we derived a high-resolution ( $0.5^\circ \times 0.5^\circ$ ) mascon (mass concentration) solution from April 2002 to August 2023, which is innovatively constrained by multisource prior information from advanced spaceborne thermal emission and reflection radiometer, satellite altimetry, and WaterGAP global hydrology model. Therefore, the developed mascon solution shows higher spatial resolution than the three state-of-the-art global mascon solutions regarding the spatial distribution of mass change trends. Moreover, our mascon solution is highly correlated with in situ measurements at four stations compared to the three mascon solutions in capturing the interannual mass variations with an average correlation coefficient of 0.60. Then, we further investigate the spatiotemporal mass change characteristics in HMA with the developed high-spatial resolution mascon solution. Results show that the Central Himalayas, Western Himalayas, and Nyainqentanglha experienced the most substantial losses from 2002 to 2023, with trends of  $5.46 \pm 0.42$ ,  $3.92 \pm 0.80$ , and  $3.79 \pm 1.20$  Gt/yr, respectively. Additionally, seasonal variations' magnitudes and temporal patterns vary with regions, exhibiting significant spatial heterogeneity. Our high-spatial resolution mascon solution provides valuable records, unveiling mass changes and potential glacier instability hidden in low-spatial resolution solutions. This enhancement strengthens the capabilities of GRACE/GRACE-FO in comprehending the global glacier response to climate change.

**Index Terms**—Gravity Recovery and Climate Experiment (GRACE), high mountain Asia (HMA), mass change, regularization, spatial resolution.

## I. INTRODUCTION

**H**IGH mountain Asia (HMA), comprising the Tibetan Plateau (TP) and its surrounding mountains, including

Manuscript received 14 March 2024; revised 23 May 2024 and 26 June 2024; accepted 13 July 2024. Date of publication 16 July 2024; date of current version 26 July 2024. This work was supported by the National Natural Science Foundation of China under Grant 42274005. (Corresponding author: Yunzhong Shen.)

Wei Wang, Yunzhong Shen, and Qiuji Chen are with the College of Surveying and Geo-Informatics, Tongji University, Shanghai 200092, China (e-mail: wangwei\_96@tongji.edu.cn; yzshen@tongji.edu.cn; qiujiachen@tongji.edu.cn).

Fengwei Wang is with the State Key Laboratory of Marine Geology, Tongji University, Shanghai 200092, China (e-mail: wangfw-foster@tongji.edu.cn). Digital Object Identifier 10.1109/JSTARS.2024.3429328

the Tien Shan, Pamir, Karakoram, and Himalaya, has the largest solid freshwater storage outside the Antarctic and Arctic [1], [2]. As global temperatures persistently increase, the mass balance of HMA has been disrupted [3]. Glaciers over HMA are retreating and undergoing sustained melting, contributing to global mean sea-level rise [4]; simultaneously, the freshwater supply originating from glacier melting has been changing, which significantly impacts the agriculture, economy, and hydropower industries of surrounding countries, including Pakistan, Tajikistan, and India [5]. Therefore, monitoring HMA glacier mass changes is paramount, considering its dual role in contributing to global sea-level change and regional water resource supplement.

Remote sensing satellite technology provides unique observations for monitoring mass changes in mountain glaciers [6]. Since March 2002, the Gravity Recovery and Climate Experiment (GRACE), and its successor, the GRACE Follow-On (GRACE-FO) satellite mission have provided more than two decades of unique observations to monitor global mass changes [6]. Given the significance of HMA, previous researchers have conducted numerous studies on its mass change using GRACE/GRACE-FO (GRACE-/FO) data [7], [8], [9], [10], [11], [12], [13], [14], [15], [16], [17]. These studies suggest a significant reduction in total mass over HMA. Nevertheless, reported mass change trends cannot be reconciled within the error bound at a regional scale despite slightly different periods. For example, in Spiti Lahaul, Xiang et al. [14] reported a mass loss of  $-2.36 \pm 0.50$  Gt/yr for 2002–2016, while Xiang et al. [15] reported only  $-0.24 \pm 0.41$  Gt/yr for 2002–2021. Moreover, Wouters et al. [18] found that there existed an underestimation of mass loss with GRACE data in Central Asia and an overestimation in South Asia East. The HMA mass change uncertainties from GRACE-/FO are primarily attributed to the coarse spatial resolution and “signal leakage” issue. The former is attributed to the orbit configuration, while the latter normally occurs when suppressing correlated errors and random noise via decorrelation filters [19], [20] and Gaussian smoothing [21], [22].

Conventionally, forward modeling algorithm [16], [23] and space domain inverse computing scheme [24] are usually applied to deal with the “signal leakage” problem [22], [25]. However, it is difficult to reveal mass changes at a finer scale with these methods, since the spatial constraint is still insufficient. Recently, Center for Space Research (CSR) of the University of Texas, Jet Propulsion Laboratory (JPL), and Goddard Space

Flight Center (GSFC) have generated their GRACE/-FO global mascon solutions with distinctive constraint strategies, which have effectively mitigated this “signal leakage” issue and improved the spatial resolution to some extent [26], [27], [28]. The nominal spatial resolution of CSR mascon, GSFC mascon, and JPL mascon is  $1^\circ \times 1^\circ$ ,  $1^\circ \times 1^\circ$ , and  $0.5^\circ \times 0.5^\circ$  over HMA, respectively. These mascon solutions have been widely used in studies over HMA [22], [29], [30], [31], [32]. Nevertheless, discrepancies persist among these three mascon solutions at the finer-scale spatial distribution of mass changes, as described in [33]. The inconsistencies primarily arise from the differences in employed spatial constraints: CSR relies solely on GRACE information, and GSFC employs spatially correlated exponential function; JPL mascon adopts the Global Land Data Assimilation System (GLDAS) Noah model as prior information for spatial constraints over HMA. However, there are complex components in mass changes over HMA (e.g., glacier, lake, soil moisture changes) [17], which cannot be accurately simulated in Noah leading to the inaccurate constrain of JPL mascon [33]. As a result, despite being state-of-the-art GRACE mascon products, these three mascon solutions still cannot meet the demands for characterizing finer-scale glacier changes over HMA. Moreover, the comparison between GRACE estimates and in situ measurements is relatively lacking. These emphasize the need to develop an HMA regional high-resolution mascon solution to quantify mountain glacier mass change at finer scales.

Considering that mass changes in HMA are predominantly influenced by glacier mass changes, lake volume expansion, and soil moisture variations [31], we can enhance the spatial resolution of the GRACE/-FO mascon solution by using prior information in this region. Compared to those three global mascon solutions, we applied comprehensive spatial constraint by introducing multisource prior information with a much higher spatial resolution for complex mass change components. In this study, we introduce three types of high spatial resolution prior information into HMA mascon modeling via a regularization matrix and derive a  $0.5^\circ \times 0.5^\circ$  mascon solution from April 2002 to August 2023. Notably, this solution exclusively relies on the GRACE/-FO observations, with external high-spatial resolution from the prior information constraints. Consequently, our solution retains the GRACE/-FO signals while effectively addressing challenges related to “signal leakage” and low resolution.

The rest of this article is organized as follows: Section II briefly introduces the study area and the used data, including the GRACE/GRACE-FO gravity field model and multisource high-resolution prior information. Section III presents the methodologies of the high-resolution mascon solution, and Section IV shows the performance of the developed mascon solution and evaluates the corresponding results. Then the spatiotemporal analysis of mass changes is shown in Section V. Discussions and conclusions are shown in Sections VI and VII.

## II. MATERIAL

### A. Study Area

Known as Earth’s Third Pole and Asian Water Tower [34], HMA spans the Altai and Tien Shan mountains to the TP

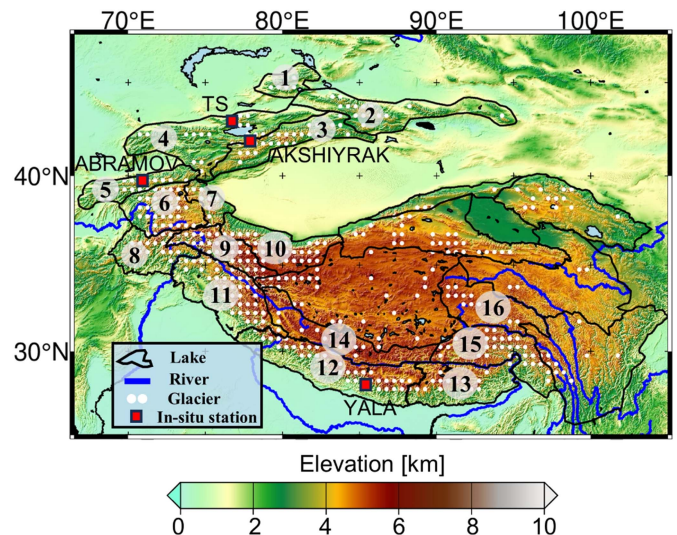


Fig. 1. Map of the HMA with topography. Names of the HiMAP regions are as: 1. Dzhungarsky Alatau, 2. Eastern Tien Shan, 3. Central Tien Shan, 4. Northern Western Tien Shan, 5. Pamir Alay, 6. Western Pamir, 7. Eastern Pamir, 8. Eastern Hindu Kush, 9. Karakoram, 10. Western Kunlun Shan, 11. Western Himalaya, 12. Central Himalaya, 13. Eastern Himalaya, 14. Gangdise Mountains, 15. Nyainqentanglha, 16. Tanggula Shan. TS is short for TS.TUYUKSUYSKIY.

from north to south at  $65^\circ$ – $105^\circ$ E and  $26^\circ$ – $47^\circ$ N. Located in the heart of Asia, HMA is surrounded by many glaciers and lakes, making it the source of major rivers in Asia, such as the Indus, Ganges, and Yangtze. Fig. 1 shows the topography of HMA and major waterways over this region. According to the region definition from Himalayan Monitoring and Assessment Programme (HiMAP) [35], HMA is divided into 23 regions, as shown in Fig. 1. There are glaciers inventoried in the Randolph Glacier Inventory (RGI v6.0) [2] over HMA, covering an area of  $97605 \pm 7935$  km<sup>2</sup> [36]. The positions of glaciers from RGI 6.0 are marked with white dots at a  $0.5^\circ \times 0.5^\circ$  spatial resolution [37]. Throughout this study, we highlight 16 regions with significant glacier coverage, labeled in Fig. 1.

### B. GRACE and GRACE-FO Product

The monthly Tongji-Grace2022 gravity field product from April 2002 to August 2023 with the spherical harmonic coefficients (SHCs) up to degree and order of 96 [38] is used to construct the observation equations for our mascon solutions. Since degree-one coefficients are not available in the Tongji-Grace2022 product, we added back degree-one terms with those from Technical Note-13.CSR [39], [40]. All  $C_{20}$  and  $C_{30}$  (after August 2016) coefficients are replaced with corresponding values from satellite laser ranging solutions [41]. Three state-of-the-art global mascon solutions from CSR, JPL, and GSFC are used for comparison [27], [28], [42].

### C. High-Spatial Resolution Multisource Information

The high-spatial-resolution long-term and seasonal mass change signals from multisource information are used as the spatial constraint of our monthly mascon solution. The input and

TABLE I  
INPUT AND OUTPUT DATASETS

	Datasets	Purpose	Time span used
Input	Tongji-Grace2022	Observation	2002.04–2023.08
	Lake water storage change from altimetry	Constraint	2002.04–2017.12
	Hydrological simulation from WGHM	Constraint	2002.04–2017.12
	Glacier mass balance from ASTER	Constraint	2002.04–2017.12
Output	High-spatial resolution mascon solution	Result	2002.04–2023.08

output datasets, along with their corresponding purposes and the time spans used for generating the high-spatial-resolution mascon solution, are summarized in Table I.

The lake water storage change accounts for an essential component of HMA mass changes, we include the water storage change time series of 52 lakes over the TP from 2002 to 2017, provided by Li et al. [43] for spatial constraint. As the provided datasets are submonthly, we smoothed the time series using a one-month moving average filter to generate monthly datasets same as GRACE/-FO products. These datasets were derived from multiple altimetric missions and Landsat-derived lake shoreline positions. The lake water storage change information outside TP was added with datasets from Liao et al. [44]. Finally, they are standardized to a spatial resolution of  $0.5^\circ \times 0.5^\circ$  for this study. In contrast to land surface models, WaterGAP incorporates anthropogenic water use, including irrigation, manufacturing, and livestock farming [45]. Hence, the information on the other hydrological components (soil moisture, groundwater, rivers, reservoirs, snow, canopy storage, global wetlands, and local wetlands) from 2002 to 2017 are obtained from  $0.5^\circ \times 0.5^\circ$  gridded WaterGAP global hydrology model (WGHM) version 2.2e.<sup>1</sup>

The monthly glacial mass change estimates from the digital elevation model differencing over HMA from 2002 to 2019 are used in this study. The datasets are provided by Hugonnet et al. [46] in the form of  $0.5^\circ \times 0.5^\circ$  tiles, in which the glacial elevation changes are first derived from NASA's archive of stereo images from the Advanced Spaceborne Thermal Emission and Reflection Radiometer (ASTER). Therefore, the datasets have much higher spatial resolution than GRACE/-FO observations. It should be noted that the tectonic effects (such as the uplift of the TP) and nontectonic effects (such as the surface loading deformation of the region) did not significantly affect the estimation of the glacier volume changes because there is no statistically significant bias in glacier volume changes over HMA, as validated in [46]. Then, the elevation change over each inventoried glacier multiplies the glacier coverage and yields glacier volume change. Finally, the glacier mass changes in the form of equivalent water height are obtained by multiplying the assumed glacier density from Huss [47]. When establishing the spatial constraint of glacier mass changes, we used ASTER data

from 2002 to 2017 to be consistent with the period of the lake storage information.

### III. METHODOLOGY

#### A. Preparation for High-Resolution Mascon Model

To address the challenge that the low-spatial resolution of GRACE/-FO products limits its capability to accurately estimate global mountain glacier mass changes, we attempt to incorporate high-resolution multisource prior information into the mascon solution over HMA. Before this, two aspects need clarification. First, it is essential to show the consistency between the Tongji-Grace2022 product and high-spatial-resolution prior information data in capturing the dominant mass change signals. Second, it is necessary to illustrate the disparity in spatial resolution between the prior information and Tongji-Grace2022 product, to show the necessity for constraining Tongji-Grace2022 products with high-spatial resolution prior information.

For the first aspect, we employed a DDK5 filter to reduce correlation errors [20] and 200-km Gaussian smoothing [21] to suppress high-frequency noise in the Tongji-Grace2022 product up to a degree/order of 96. The same process is conducted for multisource prior information for consistency. Then, we derived the linear trend and annual amplitude by fitting the monthly mass change time series per grid for a given period with the offset, trend, annual and semi-annual terms using the least-squares method (April 2002–August 2023 for Tongji-Grace2022 product; April 2002–December 2017 for the high-spatial-resolution prior information). Subsequently, we show the long-term linear trends and annual amplitudes obtained from the Tongji-Grace2022 product in Fig. 2(a) and (b) and multisource high-resolution prior information in Fig. 2(c) and (d). For the second aspect, we calculate the Root Mean Square (RMS) of monthly mass changes from the high-spatial-resolution prior information datasets (April 2002–December 2017) and the Tongji-Grace2022 product (April 2002–August 2023) for each grid over HMA and its surroundings. RMS values are shown in Fig. 3(a)–(d) to demonstrate the spatial distributions of signal strengths.

As shown in Fig. 2, the results demonstrate good consistency between the Tongji-Grace2022 product and the high-spatial-resolution prior information at the spatial scale of native GRACE/-FO resolution ( $\sim 300$  km for monthly solutions [6]). Simultaneously, it is obvious that the spatial resolution of the prior information in Fig. 3(a)–(c) is much higher than that of the Tongji-Grace2022 product in Fig. 3(d). Therefore, we can reasonably constrain the GRACE/-FO mascon modeling using multiple high-resolution prior information and the spatial resolution of the generated mascon solution is expected to be improved.

#### B. High-Spatial Resolution Mascon Modeling

The developed framework for high-spatial-resolution mascon modeling over HMA is shown in Fig. 4(a–f), which is composed of three parts: The first part is basic mascon modeling (a–c); the second part plays an essential role in improving the spatial

1.[Online]. Available: <https://doi.org/10.5281/zenodo.10026943>.

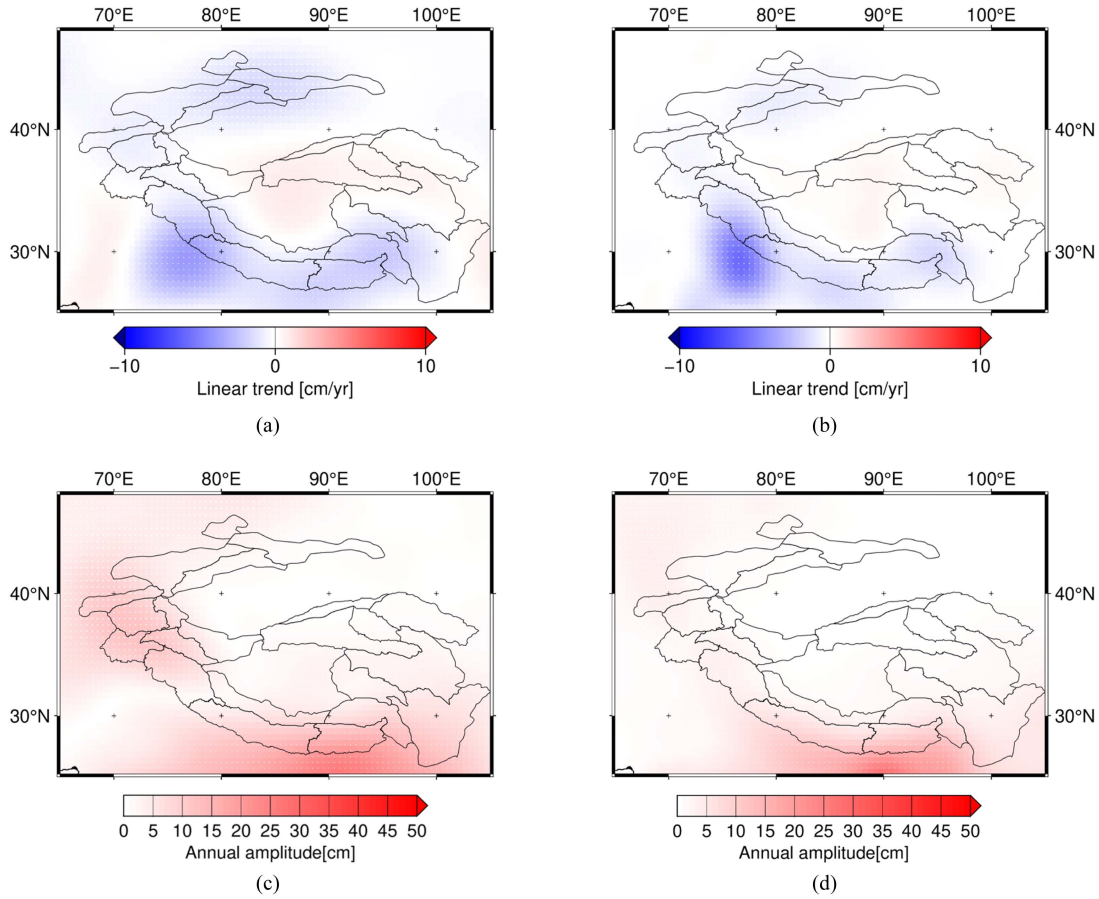


Fig. 2. Consistency assessment between the Tongji-Grace2022 product and prior information at the spatial scale of GRACE/FO native resolution over HMA and its surroundings. Spatial distribution of linear trends from (a) the Tongji-Grace2022 product and (b) prior information; annual amplitudes from (c) the Tongji-Grace2022 product and (d) prior information.

resolution of the mascon solution and addressing the challenge of accurately estimating mountain glacier mass changes. It involves the processing of multisource high-spatial resolution prior information and the construction of constraint matrices and their integration (d–e); and finally, the high-spatial-resolution mascon estimates are derived through regularization in step (f).

The basic mascon observation equation can be constructed as

$$\mathbf{y} = \mathbf{A}\mathbf{x} + \mathbf{e} \quad (1)$$

where  $\mathbf{A}$  is the  $n \times t$  design matrix,  $\mathbf{x}$  contains the unknown parameters of mass variations, and  $\mathbf{e}$  is the random error vector with a zero mean and a covariance matrix of  $\sigma_0^2 \mathbf{P}^{-1}$ .  $\sigma_0^2$  is the variance of the unit weight, and  $\mathbf{P}$  is the weight matrix of  $\mathbf{y}$ , which plays an important role in removing the correlated errors of GRACE/FO SHCs. In the basic mascon approach, the sample spatial grids at ground (mascon grids) and satellite altitude (pseudo-observations) should be determined. To reflect detailed mass variations spatially, we set the mascon sampling density at  $0.5^\circ$  (the same as those of the high spatial resolution prior information), which is finer than the native resolution of GRACE/FO products. The sampling density of pseudo-observations is set at  $0.4^\circ$ . As shown in Fig. 4(b), the design matrix  $\mathbf{A}$  of the observational equation is derived from

Newton’s law of gravitation [48]

$$\mathbf{A}(i, j) = \frac{G(\rho - d(\theta_j)\rho \cos\psi_{i,j})}{(d(\theta_j)^2 + \rho^2 - 2d(\theta_j)\rho \cos\psi_{i,j})^{3/2}} \quad (2)$$

where  $G$  is the gravitational constant,  $\rho$  is the radial distance of the  $i$ th space location,  $\theta_j$  is the colatitude of the  $j$ th mascon grid,  $d(\theta_j)$  denotes the radial distance of the  $j$ th mascon grid with ellipsoid correction [49],  $\psi_{i,j}$  is the spherical distance between the  $j$ th mascon grid and  $i$ th space location. The pseudo-observation  $\mathbf{y}$  is derived from the SHCs of GRACE/FO products, and the  $i$ th element of the observation vector denotes gravitational disturbance at  $i$ th space point.

Since (1) is ill-conditioned, the Tikhonov regularization [50] is used to solve the mascon solution with the cost function of

$$\Phi(\mathbf{x}) = (\mathbf{y} - \mathbf{A}\mathbf{x})^T \mathbf{P}(\mathbf{y} - \mathbf{A}\mathbf{x}) + \alpha \mathbf{x}^T \mathbf{R}\mathbf{x} \quad (3)$$

where the regularization parameter  $\alpha$  ( $\alpha > 0$ ) plays an important role and it is determined with the minimum mean squared error criterion [51], [52];  $\mathbf{R}$  denotes the positive definite regularization matrix, which is crucial to constrain the mascon solution as it can provides high-spatial-resolution prior information of the signal strength for each mascon parameter [53], [54].

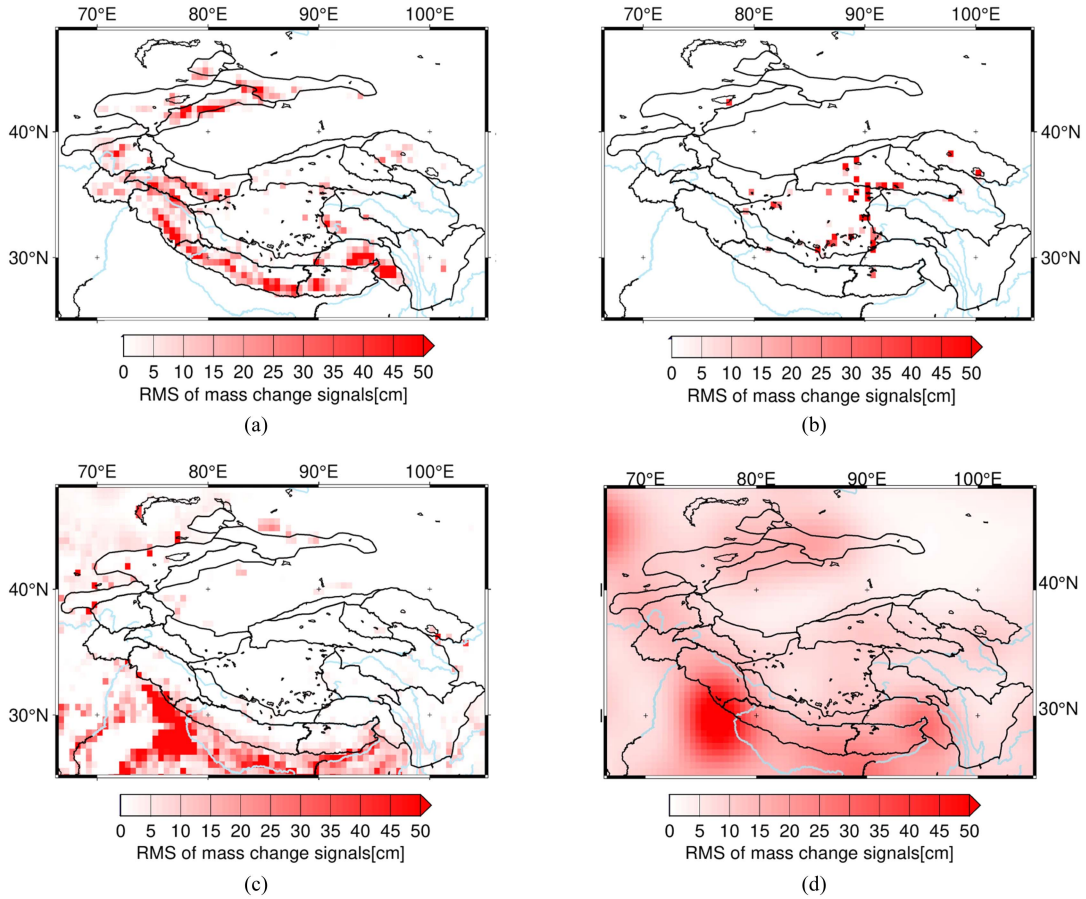


Fig. 3. Spatial distribution of RMS of (a) glacier mass change signals, (b) lakes, (c) hydrological signals excluding lakes, and (d) total mass change signals from the Tongji-Grace2022 product over HMA and its surroundings.

After the regularization parameter and regularization matrix  $\mathbf{R}_{\text{pre}}$  are determined (the construction of  $\mathbf{R}_{\text{pre}}$  is shown subsequently), we can derive the preliminary regularized solution  $\mathbf{x}_{\alpha}$  through minimizing the cost function in (3) as

$$\mathbf{x}_{\text{pre}} = (\mathbf{A}^T \mathbf{P} \mathbf{A} + \alpha \mathbf{R}_{\text{pre}})^{-1} \mathbf{A}^T \mathbf{P} \mathbf{y} \quad (4)$$

with  $\mathbf{N} = \mathbf{A}^T \mathbf{P} \mathbf{A}$ .

As noted by Save et al. [26], the shorter-term variations may be affected by linear trend terms. To this end, the mascon modeling is then refined by updating the observation equation, involving the removal of the linear trend and the application of a time-variable regularization matrix. The linear trend is derived by fitting the monthly mass change time series per mascon grid from April 2002 to August 2023 with the offset, trend, annual, and semi-annual terms using the least-squares method. The updated observation equation is

$$\mathbf{y} - \mathbf{A} \mathbf{x}_{\text{trend}} = \mathbf{A} \mathbf{x}_{s_v} + \mathbf{e} \quad (5)$$

where  $\mathbf{x}_{\text{trend}}$  denotes the linear trend terms of mass change and  $\mathbf{x}_{s_v}$  represents the short-scale mass variations.  $\mathbf{x}_{s_v}$  can be derived with  $\mathbf{x}_{s_v} = (\mathbf{A}^T \mathbf{P} \mathbf{A} + \alpha \mathbf{R}_{s_v})^{-1} \mathbf{A}^T \mathbf{P} \mathbf{y}$  in which  $\mathbf{R}_{s_v}$  is the time-variable regularization matrix for the current month (the construction of  $\mathbf{R}_{s_v}$  is shown subsequently). Finally, the high-spatial-resolution mascon solution is derived by

integrating the long-term mass change component ( $\mathbf{x}_{\text{trend}}$ ) from the preliminary solutions and the shorter-term mass variations ( $\mathbf{x}_{s_v}$ ) from the refined solutions.

The high-spatial-resolution prior information on mass changes is introduced to establish a comprehensive spatial constraint. In the preliminary mascon modeling, we derive the regularization matrix as  $\mathbf{R}_{\text{pre}} = \mathbf{R}_{\text{Glacier}} + \mathbf{R}_{\text{Lake}} + \mathbf{R}_{\text{Hydro}}$ , where the diagonal matrices  $\mathbf{R}_{\text{Glacier}}$ ,  $\mathbf{R}_{\text{Lake}}$ , and  $\mathbf{R}_{\text{Hydro}}$  reflect the spatial distribution characteristics of mass change signals. As shown in Fig. 4(c), the diagonal elements of  $\mathbf{R}_{\text{Glacier}}$ ,  $\mathbf{R}_{\text{Lake}}$  and  $\mathbf{R}_{\text{Hydro}}$  are determined with the correspondent prior signal variances  $\sigma_i^2$  ( $1 \leq i \leq t$ ) in which  $\sigma_i$  is the RMS of the mass change time series at  $i$ th mascon grid from 2002 to 2017. In the refined mascon modeling, we construct 12 regularization matrices  $\mathbf{R}_{s_v}(\text{mon})$  (where mon represents each month from January to December) to describe the spatial distribution characteristics of the refined mass change signals of each month, which is determined using the equation  $\mathbf{R}_{s_v}(\text{mon}) = \mathbf{R}_{\text{Glacier}_{s_v}}(\text{mon}) + \mathbf{R}_{\text{Lake}_{s_v}}(\text{mon}) + \mathbf{R}_{\text{Hydro}_{s_v}}(\text{mon})$ , for example,  $\mathbf{R}_{s_v}(\text{Jan.})$  is constructed with the prior signal variances derived from the detrended mass change time series only in January for 2002–2017.

As shown in Fig. 2, the dominant mass change signals, mainly the linear trends and annual signals, exhibit good consistency between 2002–2023 (Tongji-Grace2022) and 2002–2017 (prior

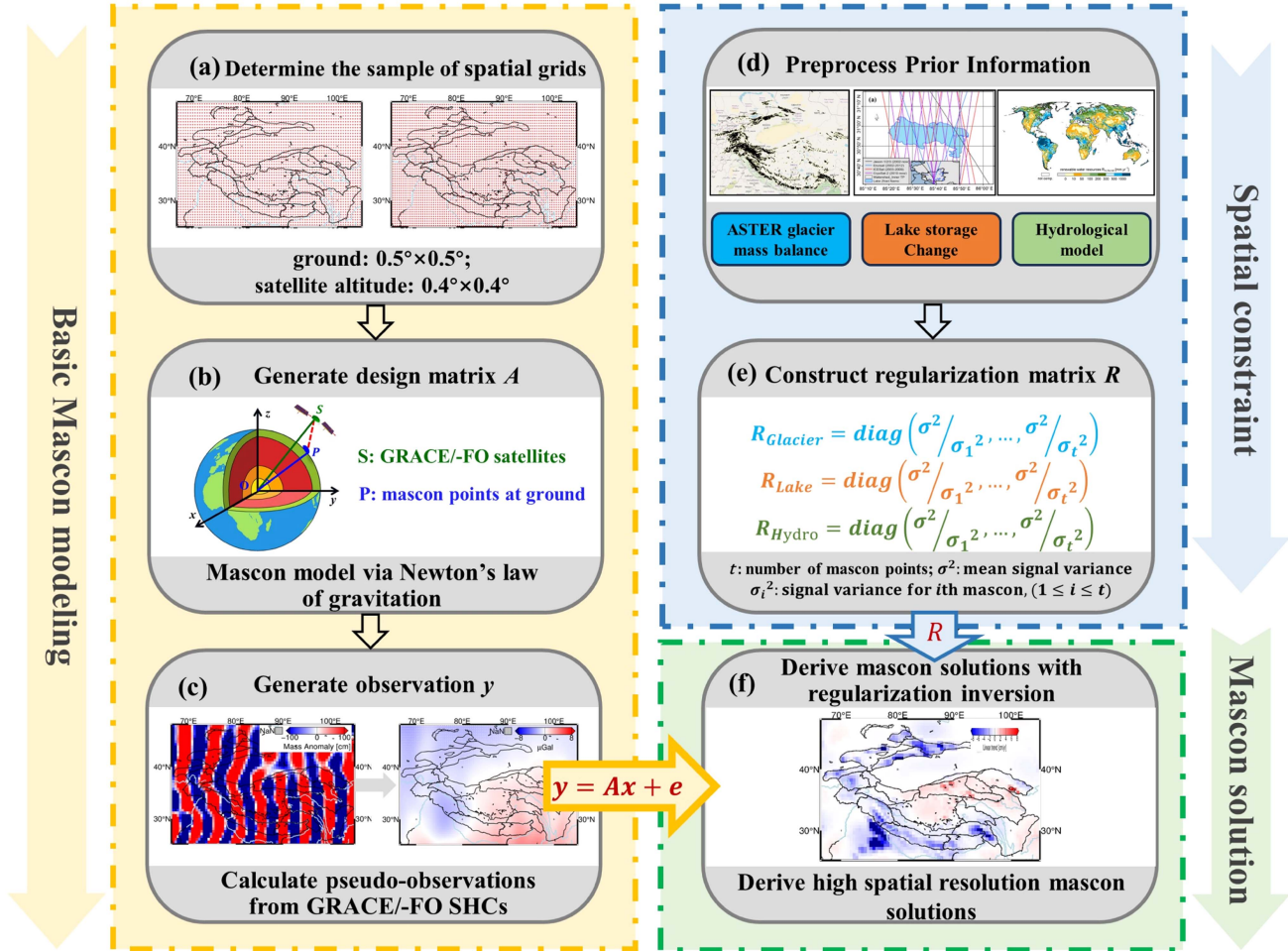


Fig. 4. Flowchart for the high-spatial-resolution mascon modeling over HMA.

information). Hence, it is reasonable to spatially constrain the mascon solution for 2002–2023 with the prior information only derived from the high-spatial-resolution data from 2002 to 2017. In practice, the regularization matrix remains the same for all months in the preliminary mascon modeling, and in the refined mascon modeling, the same regularization matrix is used for the same month across all years (with 12 regularization matrices corresponding to the months from January to December). Therefore, we can develop a high-spatial-resolution mascon solution for the time span of the Tongji-Grace2022 (from April 2002 to August 2023), even though the high-resolution prior information is only derived with the data until 2017.

### C. Glacier Mass Change Signal Extraction

To obtain the glacier mass changes over HMA, the soil moisture mass changes are removed with the GLDAS Noah data [55]. The glacial isostatic adjustment (GIA) signal is removed with the ICE-6G\_D model [56]. In this study, the linear trend is determined by fitting the mass change time series with the offset, linear trend, and annual and semi-annual terms using the least-squares method [12]. The error for the linear trend at a 95% confidence level is derived from the law of error propagation

based on the fitting error and estimated GIA error. The GIA error is estimated as the standard deviation between the three global GIA models [57] from Peltier et al. [56], Caron & Ivins [58], and Wang et al. [59].

## IV. PERFORMANCE OF MASCON SOLUTIONS

Using the developed high-spatial resolution mascon modeling, we developed a  $0.5^\circ \times 0.5^\circ$  monthly mascon solution over HMA from April 2002 to August 2023, almost four years longer than the records of ASTER. In this section, we first used the ASTER estimates to show the spatial performance of the developed mascon solution and that of the three state-of-the-art mascon solutions from CSR, JPL, and GSFC (short by CSR-M, JPL-M, and GSFC-M). The evaluation of the four mascon solutions and the ASTER estimates is conducted using in situ measurements.

### A. Comparison With the ASTER Estimates

We first show the spatial performance of the four mascon solutions over the 16 studied regions. Specifically, we estimated the glacier mass change trends of 16 regions using CSR-M, JPL-M, and GSFC-M and the developed high-spatial resolution

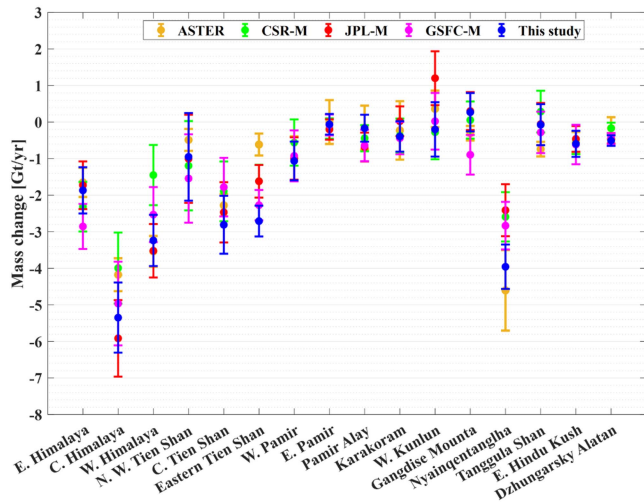


Fig. 5. Glacier mass change trend derived from mascon solutions and ASTER estimates from 2002 to 2019.

TABLE II  
RESULTS OF THE LINEAR REGRESSION FITTING BETWEEN THE MASS CHANGE TRENDS FROM MASCON AND ASTER

Mascon solution	Slope	Intercept	$R^2$
CSR-M	0.62	-0.30	0.66
JPL-M	0.95	-0.40	0.73
GSFC-M	0.73	-0.52	0.68
This study	0.97	-0.26	0.81

mascon solution from 2002 to 2019, as presented in Fig. 5. The ASTER-derived glacier mass change trends [46] during the same period are included for comparison. Then, we conducted a linear regression analysis with ASTER results on the  $x$ -axis and the mascon results on the  $y$ -axis. The corresponding fitting results are summarized in Table II. Overall, in the 16 regions, the glacier mass change trends derived from four mascon solutions align well with the ASTER estimates. The result from our high-spatial resolution mascon solution is closest to ASTER estimates, with the highest  $R^2$  (coefficient of determination) of 0.81, the largest slope of 0.97, and the smallest absolute intercept of 0.26, indicating that the bias between estimates from our mascon solution and the ASTER estimates are the smallest as we include ASTER information in the generation of our mascon solution.

Furthermore, we compared the distribution of long-term glacier mass change trends (2002 – 2019) at a spatial scale of  $0.5^\circ$  grid over the 16 regions based on four mascon solutions and ASTER in Fig. 6. Scatter density plots of linear regression analysis (ASTER estimates on the  $x$ -axis and mascon estimates on the  $y$ -axis) and the fitting results are also presented in Fig. 6. Compared to CSR-M, GSFC-M, and JPL-M, the slope and  $R^2$  between our high-spatial resolution mascon solution and ASTER are much higher (slope = 0.59 and  $R^2 = 0.43$ ), indicating that our solution is closer to ASTER estimates and the spatial resolution is significantly improved.

From Fig. 6, it is evident that most of the 16 regions over HMA exhibit negative trends, indicating long-term glacier mass loss. Compared to CSR-M, GSFC-M, and JPL-M, the developed mascon method can concentrate the mass changes in areas with dense glacier distribution, while significantly weakening the signal in regions where glaciers are sparsely distributed. This indicates an improvement in the spatial resolution in mass change estimates. The spatial distributions of JPL-M, our high-resolution mascon, and ASTER estimates from reference [60] show the mass gain signals in the Western Kunlun Shan region, which are scarcely evident in the CSR-M and GSFC-M results. This discrepancy may be attributed to the lower spatial resolution of the CSR-M and GSFC-M solutions, potentially submerging the detailed signals. The glacier mass change trends from CSR-M and GSFC-M products exhibit a widespread spatial distribution owing to limited resolution. Notably, three significant loss areas are evident, specifically at the junction of the Western and Central Himalayas, the Nyainqentanglha region, and the Central Tien Shan. However, mascon solutions with additional external constraints, i.e., JPL-M and our developed mascon solution, unveil more detailed signals. For example, mass loss signals are observed at the junction of the Central and Eastern Himalayas and in the Western Pamirs. Compared to JPL-M results, ours show finer glacier melting signals, particularly in the Tien Shan region. Furthermore, the spatial distribution of the glacier melting signal in the Himalayan region is accurately rectified in the results from our solution, credited to the high-resolution spatial constraints provided by ASTER [61].

### B. Evaluation With the In Situ Measurements

Here, we used the glacier mass changes in the form of equivalent water height changes (cm), provided by WGMS (world glacier monitoring service) from in situ measurements at YALA, TS (TS.TUYUKSUYSKIY), AKSHIYRAK, and ABRAMOV stations (locations are shown in Fig. 1) to evaluate the performance of the four mascon solutions and the ASTER data. These stations are located within specific altitude ranges, with spatial scales much smaller than that of the ASTER and mascon grid. Consequently, direct comparison of long-term mass change trends or fluctuations becomes challenging. Thus, we detrend the time series of annual mass change from in situ measurement to obtain the interannual mass variations. For the monthly mass change time series of four mascon solutions and ASTER data, we applied detrending and subsequently smoothed them using a 13-month moving average filter to derive the interannual mass variations. The interannual mass variations and the correlation coefficients with the in situ measurements are shown in Fig. 7 and Table III, respectively.

All four in situ stations show significant year-to-year fluctuations in mass changes with distinctive temporal patterns, despite in situ results surpassing those derived from GRACE/-FO products in magnitude due to the deliberate placement of measurement stations in areas characterized by pronounced glacier loss [62]. The interannual mass change patterns from in situ measurements and mascon solutions are generally consistent at YALA, AKSHIYRAK, and ABRAMOV stations. However,

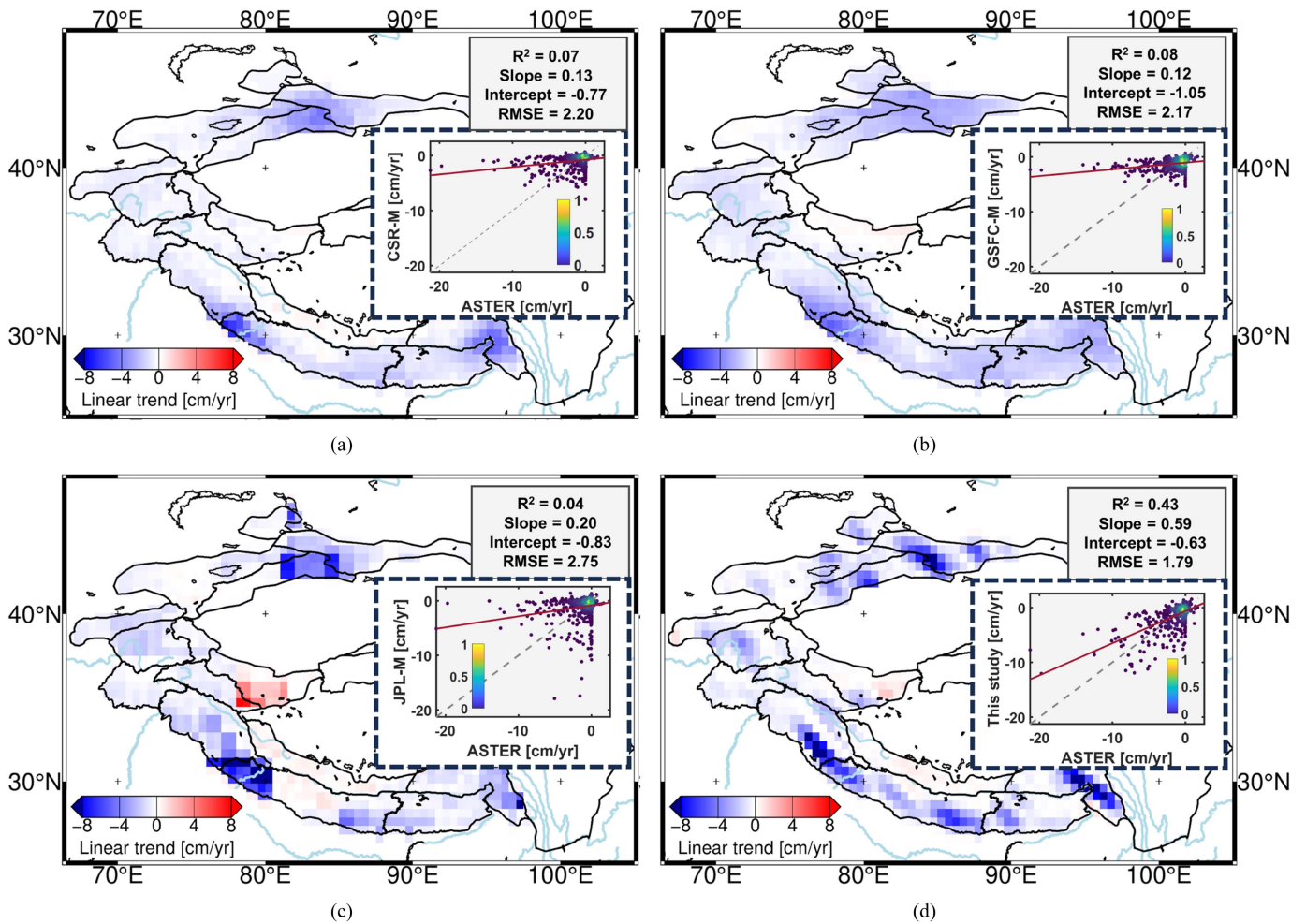


Fig. 6. Spatial distribution of the glacier mass change trends (2002–2019) derived from (a) CSR-M, (b) GSFC-M, (c) JPL-M, and (d) this study. Corresponding scatter plots with density and fitting results are presented in the enclosed subplots by dashed and solid lines, respectively.

TABLE III  
INFORMATION OF IN SITU STATIONS AND CORRELATION COEFFICIENTS OF INTERANNUAL MASS CHANGES FROM IN SITU MEASUREMENTS AND MASCON SOLUTIONS

Station name	Location (latitude, longitude)	Period	Correlation coefficient			
			CSR-M	JPL-M	GSFC-M	This study
YALA	(28.24°N, 85.61°E)	2012–2022	0.17	0.46	0.48	0.63
TS	(43.05°N, 77.07°E)	2006–2022	-0.04	-0.21	-0.04	0.55
AKSHIYRAK	(41.81°N, 78.13°E)	2011–2022	0.45	0.55	0.62	0.65
ABRAMOV	(71.57°N, 39.65°E)	2012–2022	0.33	0.50	0.31	0.56

the interannual variations from ASTER are weaker than those from GRACE/-FO mascon solutions. This is preliminary due to that the monthly ASTER time series are derived by empirical interpolation [46], rather than actual monthly observations as GRACE/GRACE-FO. Our high-resolution mascon estimates closely align with the in situ measurements at the four stations, which have notably higher correlation coefficients than those obtained from other mascon solutions (see Table III). Significantly, at the TS station, where the three mascon solutions fall short in capturing the interannual characteristics of in situ mass changes, the high-resolution mascon achieves a correlation

coefficient of up to 0.55 with the in situ data. The high-resolution mascon solution outperforms the three global ones, benefiting from both the high-accurate monthly mass change signals from GRACE/-FO observations and the constraints from high-spatial resolution distribution from the prior information.

From 2012 to 2021, the YALA station exhibited a nuanced mass fluctuation: an initial increase, followed by a decline, a gradual ascent, reaching its peak in 2021, and ultimately, a drop in 2022. The TS station, as indicated by both in situ measurements and our developed mascon solution, presented dual peaks in 2008 and 2016, respectively. Turning to



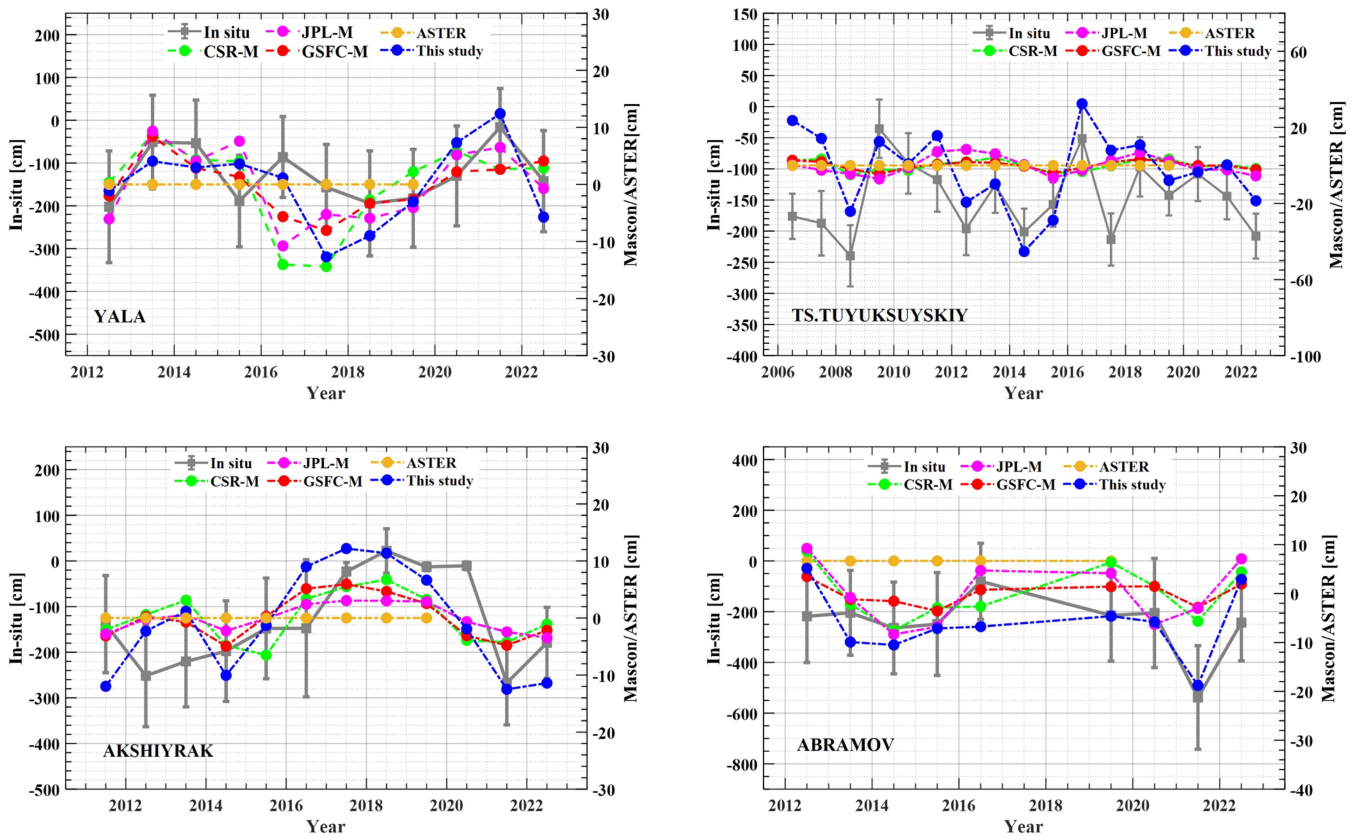


Fig. 7. Interannual mass variations were derived from the in situ measurements, GRACE/FO mascon solutions, and ASTER [46] at the four stations.

AKSHIYRAK, between 2012 and 2022, all four mascon solutions displayed a commendable correlation with in situ data, coupled with a noticeable mass gain in 2018. In the same period for AKSHIYRAK, the four mascon solutions showcased a robust correlation with in situ data, along with a conspicuous mass increase in 2018. Meanwhile, ABRAMOV experienced a notable mass decrease in 2021, confirmed by both in situ measurements and our mascon solution.

## V. RESULTS AND ANALYSIS

### A. Spatial Analysis of Long-Term Glacier Mass Change Trends From 2002 to 2023

Using the developed high-spatial resolution mascon solution, we compute the long-term trends of HMA glacier mass changes from April 2002 to August 2023. The spatial distributions and corresponding statistical histograms of long-term trends are shown in Fig. 8. The results reveal that the most severe mass loss for the study period occurs in the Himalayas, Nyainqentanglha, and Tien Shan, with maximum mass loss trends reaching 12.6, 12.0, and 9.8 cm/yr. The averaged mass change trends over the three regions are 1.8, 2.3, and 1.5 cm/yr, respectively. For these three abovementioned regions, the mass change trend differs considerably among individual mascon grids in the region; for instance, the mass change trend in the Himalayas ranges from  $-12.6$  to  $0.8$  cm/yr. These results indicate high spatial heterogeneity of mass change trends over these regions. The Pamir

& Eastern Hindu Kush and Karakoram & Kunlun Shan suffer moderate mass loss with a mean trend of  $-0.9$  and  $0.4$  cm/yr. In contrast, the mass loss over the Tangula Shan and Gangdise are relatively subdued, varying from  $-1.2$  to  $0.8$  cm/yr and  $-1.3$  to  $0.6$  cm/yr.

### B. Temporal Analysis of Mass Changes

Here, we estimate the HMA mass change time series of the four mascon solutions from April 2002 to December 2023, with the results presented in Fig. 9. Results show that the mass changes of the four mascon solutions all exhibit a pronounced loss trend, accompanied by distinct seasonal and interannual variability signals. The mass loss trends of CSR-M, JPL-M, GSFC-M, and our mascon are  $21.4 \pm 9.2$ ,  $23.3 \pm 9.2$ ,  $25.5 \pm 9.1$ , and  $25.8 \pm 9.6$  Gt/yr, respectively. Our result agrees well with those of CSR-M, JPL-M, and GSFC-M but with a higher spatial resolution (see Fig. 6), because the observations of our mascon modeling are from the GRACE/FO while high-spatial resolution information is used for spatial constraining, i.e., our method can combine the high accuracy from GRACE/FO products and high spatial resolution of the prior information.

Hence, we then calculate the averaged mass change time series of the 16 regions with the developed mascon solution, and the results are shown in Fig. 10. Notably, the Central Himalayas, Western Himalayas, and Nyainqentanglha regions exhibit the most substantial mass losses, with trends of 5.46

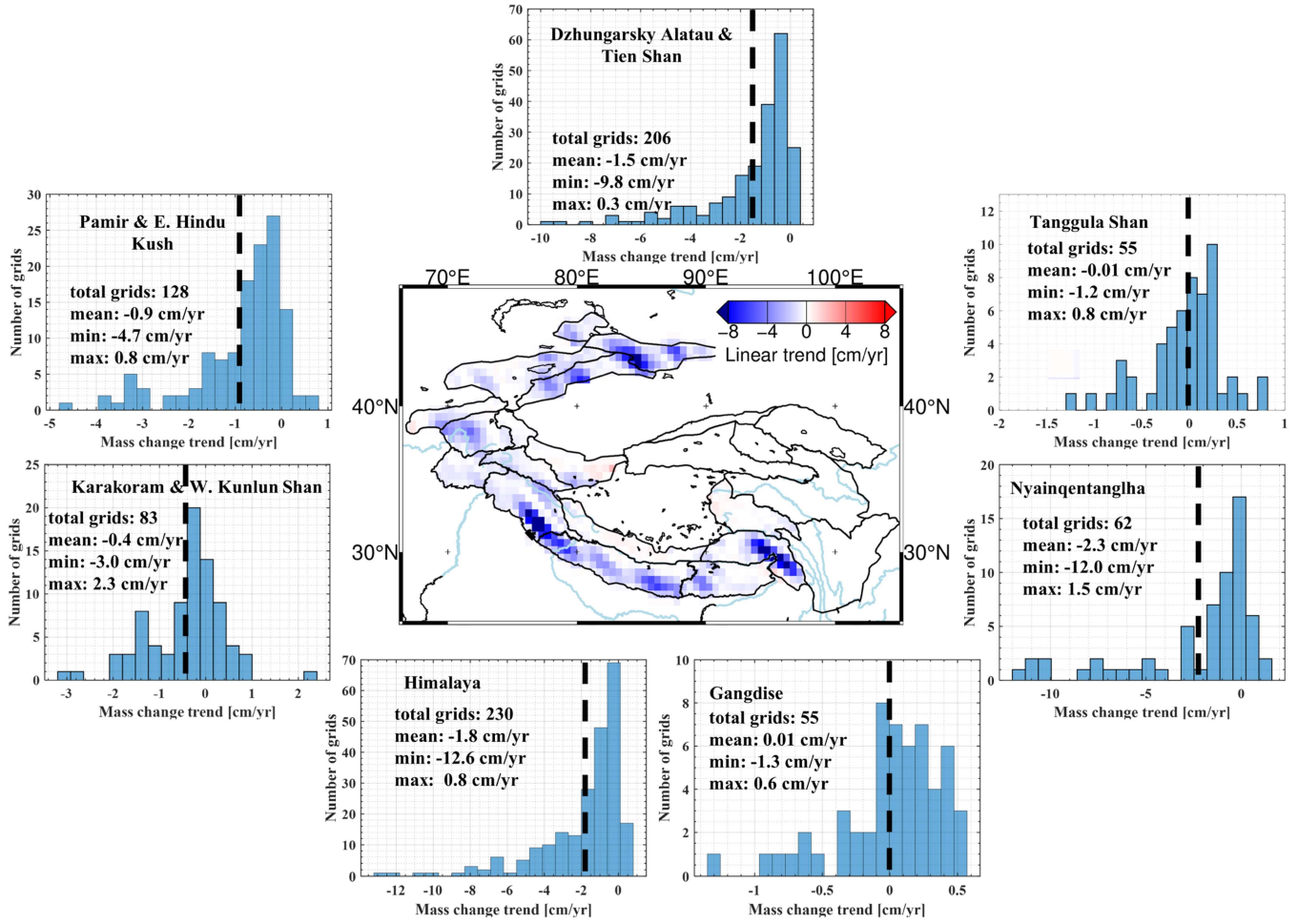


Fig. 8. Spatial distribution and corresponding statistical histograms of mass change trends over HMA from April 2002 to August 2023. The unit of “cm/yr” represents equivalent water height change in ice mass at a  $0.5^\circ \times 0.5^\circ$  grid.

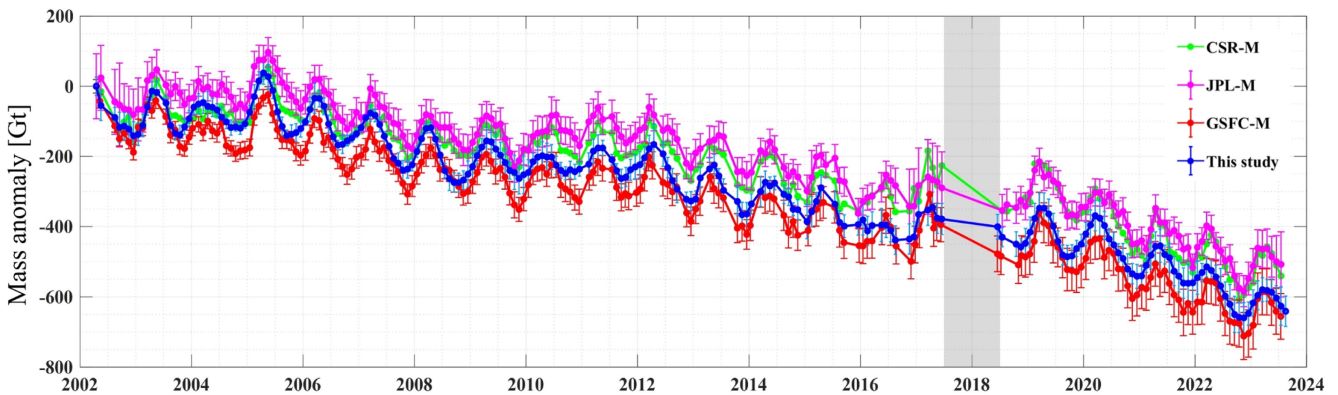


Fig. 9. Time series of mass changes over HMA from April 2002 to August 2023. The 11-month gap between GRACE and GRACE-FO is shown in gray.

$\pm 0.42$ ,  $3.92 \pm 0.80$ , and  $3.79 \pm 1.20$  Gt/yr, respectively. The three regions totally account for approximately half of the total HMA mass loss. Additionally, quasi-5-year periodic signals appear in the Northwestern Tien Shan, Central Tien Shan, Dzhungarsky Alatau, Eastern Pamir, and Western Kunlun regions, which confirmed the 5-year undulating signals revealed

by the 10-year GRACE observations from 2003 to 2013 by Yi and Sun [24]. These periodic signals may be controlled by the El Niño-Southern Oscillation and the Arctic Oscillation [24]. In the last five years, mass losses have intensified significantly in the Western Pamirs, Pamir Alay, Western Himalayas, and Gangdise regions, indicating the severity of climate change in recent years

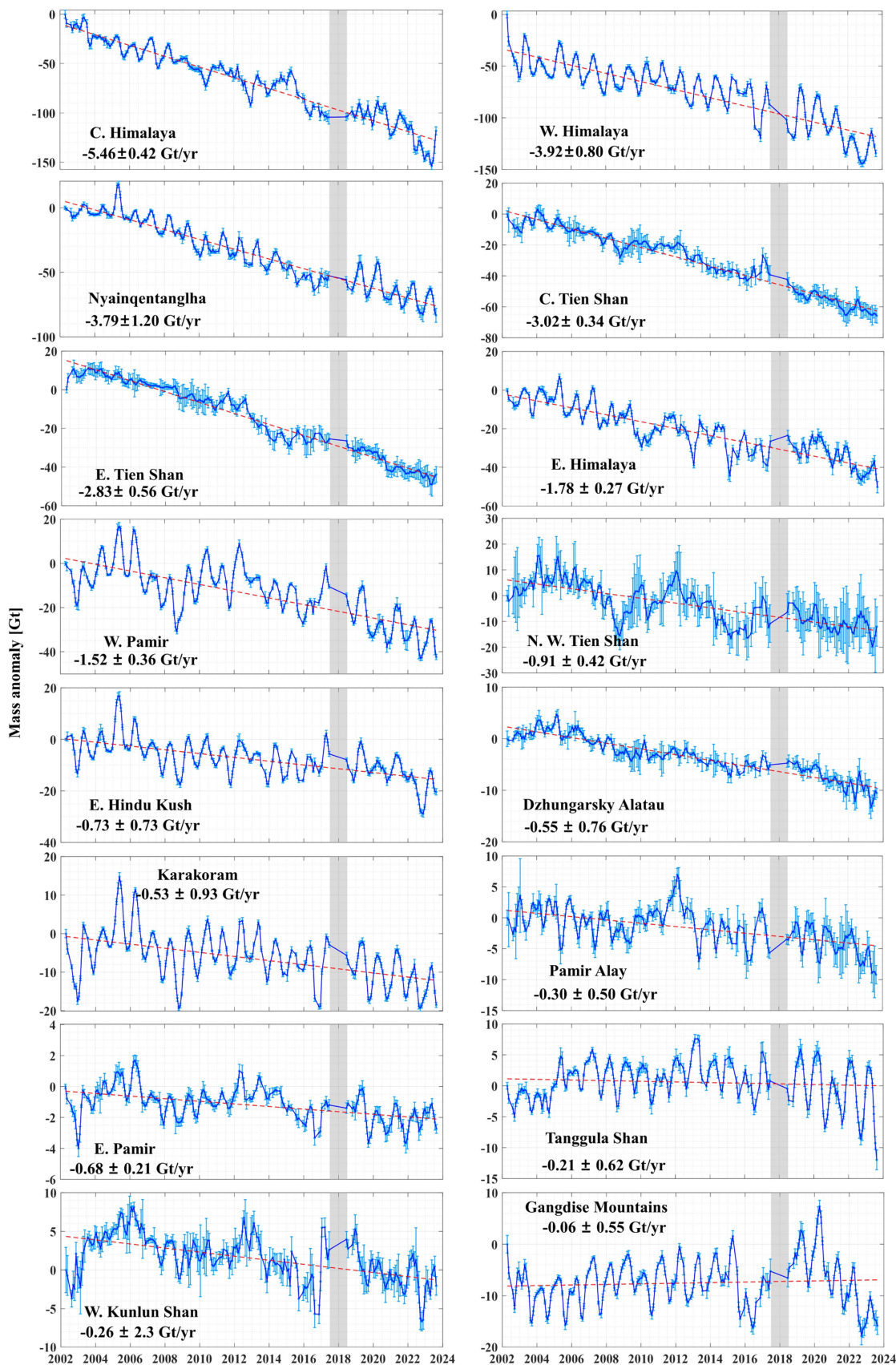


Fig. 10. Time series of mass changes for 16 regions over HMA from April 2002 to August 2023. The 11-month gap between GRACE and GRACE-FO is shown in gray. The red dashed line represents the linear trend of mass changes, while the blue dashed line represents the linear trend, along with annual and semi-annual signals.

TABLE IV  
PUBLISHED GLACIER MASS CHANGE TRENDS OVER HMA AND OUR RESULTS

Reference	Observation method	Period	Mass change trend [Gt/yr]	Our Results [Gt/yr]
Loomis et al. [17]	GRACE	2003–2016	$-23.6 \pm 5.5$	$-24.16 \pm 9.25$
Ciraci et al. [10]	GRACE/-FO	2002–2019	$-28.8 \pm 12$	$-23.48 \pm 8.91$
Matsuo & Heki [11]	GRACE	2003–2009	$-47$	$-24.44 \pm 13.85$
Jacob et al. [7]	GRACE	2003–2010	$-4 \pm 20$	$-24.98 \pm 11.89$
Schrama et al. [9]	GRACE	2003–2013	$-16.5 \pm 3.8$	$-21.15 \pm 9.88$
Wouters et al. [18]	GRACE	2003–2016	$-17.7 \pm 11.3$	$-22.98 \pm 9.28$
Liu et al. [16]	GRACE/-FO	2010–2019	$-27.3 \pm 3.1$	$-25.55 \pm 10.16$
Wang et al. [69]	GRACE/-FO +ICESat-1/2	2003–2019	$-28.0 \pm 6.0$	$-23.83 \pm 8.92$
Gardner [62]	GRACE + ICESat	2003–2009	$-26 \pm 12$	$-24.45 \pm 13.86$
Shean et al. [61]	ASTER	2000–2018	$-19.0 \pm 2.5$	$-23.94 \pm 9.1$
Li et al. [43]	ASTER	2000–2019	$-21.10 \pm 2.5$	$-23.89 \pm 9.0$
Jakob et al. [67]	CryoSat-2	2010–2019	$-28.0 \pm 3.0$	$-28.80 \pm 11.0$
Fan et al. [68]	ICESat-2	2000–2021	$-17.53 \pm 11.36$	$-23.20 \pm 8.82$
Zemp et al. [70]	In-situ	2006–2016	$-13 \pm 12$	$-23.11 \pm 9.90$

and the vulnerability of the glaciers over these regions. The Karakoram anomaly phenomenon, defined as a significant mass increase in the Karakoram and its surrounding regions [63], [64], peaked around 2006. However, the Karakoram region shows a tendency for long-term mass decline after 2010, suggesting that the well-known “Karakoram anomaly” has stopped.

### C. Annual Mass Decrease During the Ablation Period

To further investigate the seasonal mass change patterns, we illustrated the month-to-month mass variations of the 16 regions. We then estimate the ablation period and amount (average mass decrease from 2003 to 2022), where the ablation period is determined by the months with the highest and lowest values of average mass variations. The month-to-month variations, period, and amount of glacier ablation of the 16 regions are shown in Fig. 11. The results indicate distinct seasonal signals in monthly mass variations across these 16 regions, coupled with interannual variations. The summed annual mass decrease of the 16 studied glaciers is a total of 156.7 Gt, which is slightly higher than the estimation of 67–138 Gt (October 2018 to November 2020) from ICESat-2 data in [65], possibly due to different periods. Moreover, seasonal variations’ magnitudes and temporal patterns vary with regions, exhibiting significant spatial heterogeneity. Specifically, the ablation amount ranges from 1.5 to 32.0 Gt, in which Western Himalayas, Nyainqentanglha, Western Pamir, Central Himalayas, and Karakoram have an ablation amount exceeding 10 Gt. As for the temporal patterns, approximately half of the glaciers experience an ablation period starting from April to May and ending from October to November, suggesting that most glaciers are summer–autumn ablation type. In contrast, glaciers in Central Western Tien Shan and Pamir Alay undergo melting during the spring and summer seasons. The observed spatial heterogeneity in glacier mass variations may be attributed to atmospheric circulations, topographical features, and geological structure [66].

## VI. DISCUSSION

### A. Comparison With Previous Studies on Mass Changes Over HMA

Here, we compare the HMA mass change estimates from previous studies and our mascon solution. For a reasonable comparison, the linear glacier mass change trends are estimated for diverse periods as previous estimations, as shown in Table IV. The estimates from previous studies (partly) with GRACE/GRACE-FO products align well with those from the developed mascon solution within the error range, except for Matsuo and Heki [11] and Jacob et al. [7]. The result from Matsuo and Heki [11] is notably overestimated because the GIA correction is not applied, and the “signal leakage-in” from the groundwater depletion in Northern India is not separated. Jacob et al. [7] underestimated the glacier mass loss because they included the mass gain signals in the inner TP. In comparison with estimates derived from ASTER [46], [61] and satellite altimetry of CryoSat-2 [67] and ICESat-2 [68], our mascon estimates based on GRACE/GRACE-FO observations exhibit remarkable consistency. Finally, while our results match observational data within the error range, it is worth noting that the observed values somewhat underestimate the actual mass changes since the glacier mass change in the Qilian Shan regions and inner TP is not included in this study.

### B. Comparison With Previous Studies at Regional Scale Over HMA

We further compare the results of previous studies with those from our solutions at a regional scale, as shown in Fig. 12. It is evident that our results are consistent with most of the previous findings within the error bars. In the Hindu Kush, Pamir Alay & Pamir, and West Nepal, our results align well with all the listed previous studies. Notably, in the Bhutan and East Nepal regions, our estimated mass loss trends are lower than those reported by Xiang et al. [14]. However, our results are more consistent

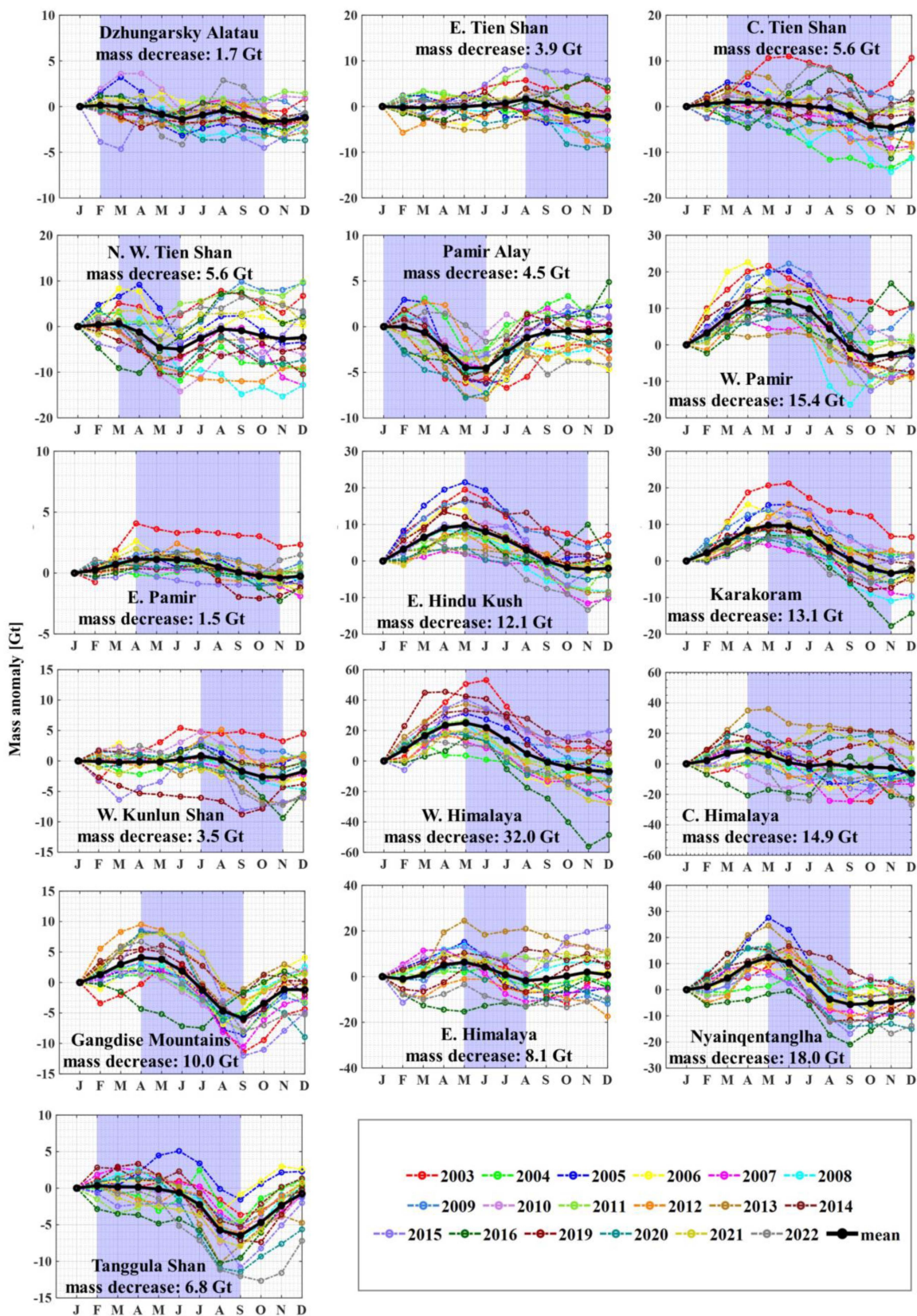


Fig. 11. Month-to-month mass variations and average ablation amounts across the 16 studied regions of HMA. The determined ablation durations are shown in purple.

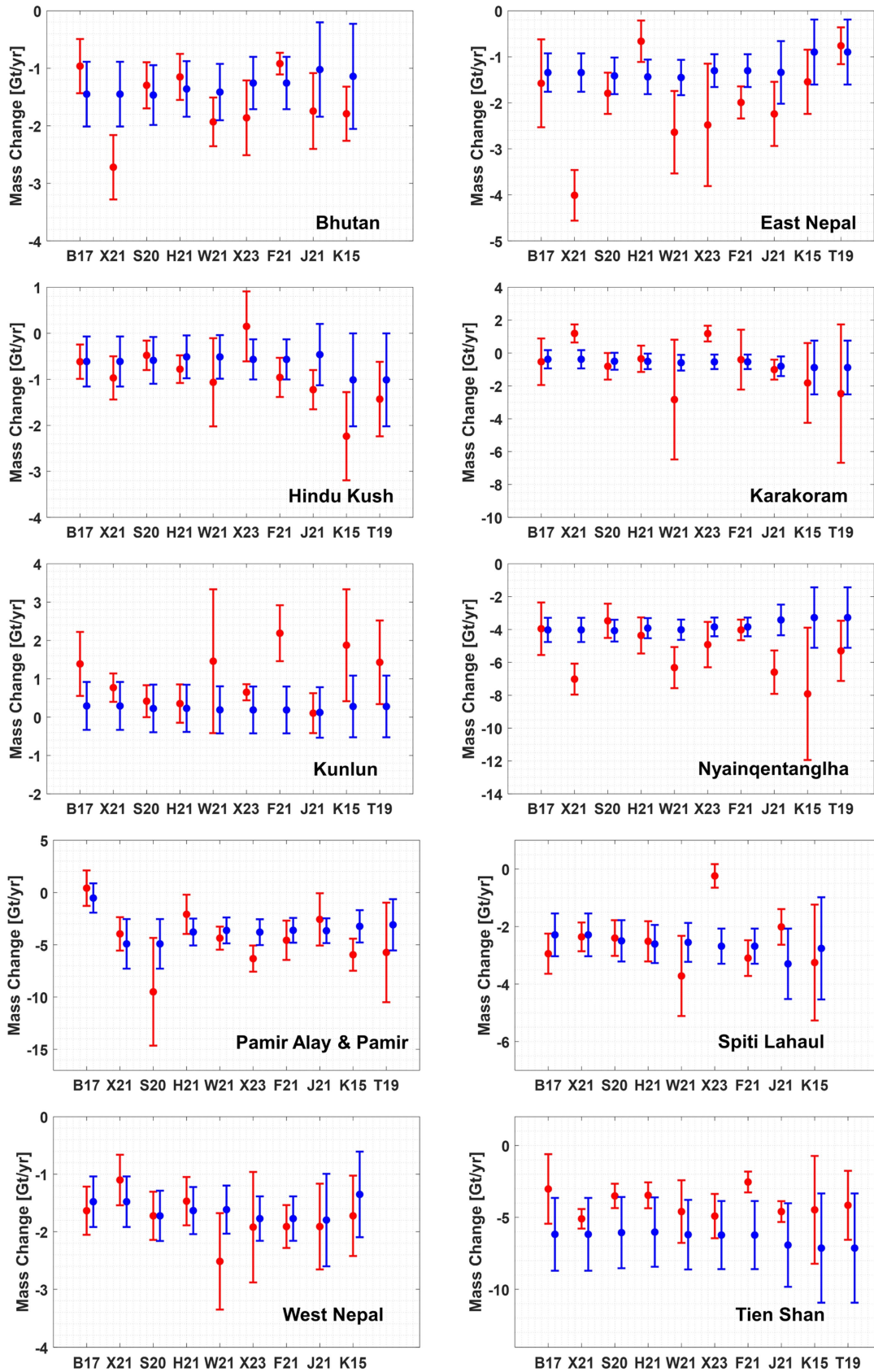


Fig. 12. HMA mass change trends at a regional level (using the regions of reference [60]) from our high-spatial resolution mascon solution (shown in blue) in comparison with previous studies (shown in red): “B17” [60], “X21” [14], “S20” [61], “H21” [46], “W21” [69], “X23” [15], “F21” [68], “J21” [67], “K15” [71], and “T19” [72]. It should be noted that the result of “K15” is completed by Jakob et al. [67] using the same method, and the results of some regions are not provided by Treichler et al. [72] since they used unique region division.

with other studies (e.g., B17 and S20), suggesting that X21 may have overestimated the mass loss trends in these two areas. Additionally, in the Karakoram, our estimates are closer to those of previous studies compared to the results of X21 and X23. In the Tien Shan, our estimated mass loss trends are consistent with other studies within the error bars. Moreover, our results in the Tien Shan are closer to those obtained by glacier modeling [73], specifically  $-6.20 \pm 2.80$  Gt/yr versus  $-7.14 \pm 3.80$  Gt/yr (ours) for 2003–2009.

## VII. CONCLUSION

This study is the first to incorporate spatial constraints from multisource prior information for developing a high-spatial-resolution monthly mascon solution over HMA from GRACE/FO products. The primary contribution is to overcome the barrier given by the limited resolution of GRACE/FO products, which prevents an accurate portrayal of mass changes over HMA mountain glaciers.

Evaluation using ASTER data and in situ measurements demonstrate that our high-spatial resolution mascon solution outperforms the three state-of-the-art global mascon solutions (CSR-M, JPL-M, and GSFC-M) in spatial and temporal mass change estimation over HMA. The linear regression fitting between results from our mascon solution and that of ASTER achieved satisfactory consistency, with a slope of 0.59 and  $R^2$  of 0.43. At the four in situ stations, our solution outperforms the other three in terms of capturing interannual mass variations compared to in situ measurements, indicating a considerable improvement of our mascon solution, notably at the TS station. Our proposed mascon solution reduces the gap between mass change estimates from GRACE/FO and other approaches through enhanced spatial resolution, adding considerably to a more unified knowledge of glacial mass changes over HMA. The enhanced spatial resolution of our solutions allows us to detect mass changes at finer scales than earlier investigations, such as Ciraci et al. [10] and Loomis et al. [17]. The spatial analysis based on the developed  $0.5^\circ \times 0.5^\circ$  grid solutions highlights that the Himalayas, Nyainqentanglha, and Tian Shan are undergoing considerable mass loss for the recent two decades, with the highest trends of 12.0, 12.6, and 9.8 cm/yr, respectively. Temporal study indicates a significant loss of  $25.8 \pm 9.6$  Gt/yr in HMA, with mass loss in the Central Himalayas, Western Himalayas, and Nyainqentanglha accounting for over half of the total. Additionally, seasonal variations' magnitudes and temporal patterns vary with regions, exhibiting significant spatial heterogeneity.

On the one hand, the high-spatial-resolution mascon solution developed over HMA provides a valuable data foundation to calibrate and validate glacier mass balance models [74]. On the other hand, this study significantly enhances the capabilities of GRACE/GRACE-FO observations in accurately estimating mountain glacier mass changes, and we unveil mass changes and potential glacier instability that remain obscured in low-resolution satellite gravimetry. Consequently, the high-resolution mascon flowchart designed for HMA can be applied to other mountain glacier regions, such as Alaska, which will play a pivotal role in advancing our comprehension of global glacier mass changes in response to climate change.

## DATA AVAILABILITY

The datasets for this research can be obtained from the following sources: HiMAP region boundary data at <https://zenodo.org/records/3600624>, the gridded glacier coverage from <https://github.com/ryanlee/RGI-Gridded.git>, the  $0.5^\circ \times 0.5^\circ$  monthly glacier mass change datasets from ASTER at <https://doi.org/10.6096/13>, the lake mass change datasets from multisatellite altimetry at <https://doi.org/10.1594/PANGAEA.898411> and <https://doi.org/10.11922/sciencedb.787>, the in situ measurements of glacier mass changes at [https://wgms.ch/data\\_databaseversions/](https://wgms.ch/data_databaseversions/), three global mascon solutions from CSR, JPL, and GSFC at [http://www2.csr.utexas.edu/grace/RL06\\_mascons.html](http://www2.csr.utexas.edu/grace/RL06_mascons.html), [https://grace.jpl.nasa.gov/data/get-data/jpl\\_global\\_mascons](https://grace.jpl.nasa.gov/data/get-data/jpl_global_mascons), and <https://earth.gsfc.nasa.gov/geo/data/grace-mascons>. The results are available upon request to the authors without any conditions.

## REFERENCES

- [1] T. D. Yao et al., "The imbalance of the Asian water tower," *Nature Rev. Earth Environ.*, vol. 3, no. 10, pp. 618–632, Oct. 2022.
- [2] R. G. I. Consortium. Randolph Glacier Inventory – "A dataset of global glacier outlines: Version 6.0: Technical report," *Glob. Land Ice Meas. Space*, Colorado, USA, 2017, doi: [10.7265/N5-RGI-60](https://doi.org/10.7265/N5-RGI-60). [Online]. Available: [https://nsidc.org/sites/nsidc.org/files/technical-references/RGI\\_Tech\\_Report\\_V6.0.pdf](https://nsidc.org/sites/nsidc.org/files/technical-references/RGI_Tech_Report_V6.0.pdf)
- [3] P. D. A. Kraaijenbrink, M. F. P. Bierkens, A. F. Lutz, and W. W. Immerzeel, "Impact of a global temperature rise of 1.5 degrees Celsius on Asia's glaciers," *Nature*, vol. 549, no. 7671, pp. 257–260, Sep. 2017.
- [4] J. T. Reager, A. S. Gardner, J. S. Famiglietti, D. N. Wiese, A. Eicker, and M. H. Lo, "A decade of sea level rise slowed by climate-driven hydrology," *Science*, vol. 351, no. 6274, pp. 699–703, Feb. 2016.
- [5] T. Bolch, "HYDROLOGY Asian glaciers are a reliable water source," *Nature*, vol. 545, no. 7653, pp. 161–162, May 2017.
- [6] B. D. Tapley et al., "Contributions of GRACE to understanding climate change," *Nature Climate Change*, vol. 9, no. 5, pp. 358–369, May 2019.
- [7] T. Jacob, J. Wahr, W. T. Pfeffer, and S. Swenson, "Recent contributions of glaciers and ice caps to sea level rise," *Nature*, vol. 482, no. 7386, pp. 514–518, Feb. 2012.
- [8] J. Y. Guo, D. P. Mu, X. Liu, H. M. Yan, Z. C. Sun, and B. Guo, "Water storage changes over the Tibetan Plateau revealed by GRACE mission," *Acta Geophysica*, vol. 64, no. 2, pp. 463–476, Apr. 2016.
- [9] E. J. O. Schrama, B. Wouters, and R. Rietbroek, "A mascon approach to assess ice sheet and glacier mass balances and their uncertainties from GRACE data," *J. Geophysical Res.-Solid Earth*, vol. 119, no. 7, pp. 6048–6066, Jul. 2014.
- [10] E. Ciraci, I. Velicogna, and S. Swenson, "Continuity of the mass loss of the world's glaciers and ice caps from the GRACE and GRACE follow-on missions," *Geophysical Res. Lett.*, vol. 47, no. 9, May 2020, Art. no. e2019GL086926.
- [11] K. Matsuo and K. Heki, "Time-variable ice loss in Asian high mountains from satellite gravimetry," *Earth Planet. Sci. Lett.*, vol. 290, no. 1/2, pp. 30–36, Feb. 2010.
- [12] T. Y. Chen, Y. Z. Shen, and Q. J. Chen, "Mass flux solution in the Tibetan Plateau using mascon modeling," *Remote Sens.*, vol. 8, no. 5, May 2016, Art. no. 439.
- [13] T. Y. Chen, J. Kusche, Y. Z. Shen, and Q. J. Chen, "A combined use of TSVD and Tikhonov regularization for mass flux solution in Tibetan Plateau," *Remote Sens.*, vol. 12, no. 12, Jun. 2020, Art. no. 2045.
- [14] L. W. Xiang, H. S. Wang, L. M. Jiang, Q. Shen, H. Steffen, and Z. Li, "Glacier mass balance in high mountain Asia inferred from a GRACE release-6 gravity solution for the period 2002–2016," *J. Arid Land*, vol. 13, no. 3, pp. 224–238, Mar. 2021.
- [15] L. W. Xiang et al., "Two decades of terrestrial water storage changes in the Tibetan Plateau and its surroundings revealed through GRACE/GRACE-FO," *Remote Sens.*, vol. 15, no. 14, Jul. 2023, Art. no. 3505.
- [16] B. S. Liu, X. C. Zou, S. Yi, N. Sneeuw, J. C. Li, and J. Q. Cai, "Reconstructing GRACE-like time series of high mountain glacier mass anomalies," *Remote Sens. Environ.*, vol. 280, Oct. 2022, Art. no. 113177.
- [17] B. D. Loomis et al., "Water storage trends in high mountain Asia," *Front. Earth Sci.*, vol. 7, Sep. 2019, Art. no. 235.

- [18] B. Wouters, A. S. Gardner, and G. Moholdt, "Global glacier mass loss during the GRACE satellite mission (2002–2016)," *Front. Earth Sci.*, vol. 7, pp. 1–11, May 2019.
- [19] S. Swenson and J. Wahr, "Post-processing removal of correlated errors in GRACE data," *Geophysical Res. Lett.*, vol. 33, no. 8, pp. 1–4, Apr. 2006.
- [20] J. Kusche, R. Schmidt, S. Petrovic, and R. Rietbroek, "Decorrelated GRACE time-variable gravity solutions by GFZ, and their validation using a hydrological model," *J. Geodesy*, vol. 83, no. 10, pp. 903–913, Oct. 2009.
- [21] J. Wahr, M. Molenaar, and F. Bryan, "Time variability of the Earth's gravity field: Hydrological and oceanic effects and their possible detection using GRACE," *J. Geophysical Res.-Solid Earth*, vol. 103, no. B12, pp. 30205–30229, Dec. 1998.
- [22] M. L. He, Z. Li, W. P. Jiang, Y. J. Pan, J. S. Jiao, and Y. X. Xiao, "Seasonal and interannual fluctuations of glacier mass balance and climate response processes on the Tibetan Plateau based on GRACE/GRACE-FO," *IEEE Trans. Geosci. Remote Sens.*, vol. 61, 2023, Art. no. 4301709.
- [23] J. L. Chen, C. R. Wilson, J. Li, and Z. Z. Zhang, "Reducing leakage error in GRACE-observed long-term ice mass change: A case study in West Antarctica," *J. Geodesy*, vol. 89, no. 9, pp. 925–940, Sep. 2015.
- [24] S. Yi and W. K. Sun, "Evaluation of glacier changes in high-mountain Asia based on 10 year GRACE RL05 models," *J. Geophysical Res.-Solid Earth*, vol. 119, no. 3, pp. 2504–2517, Mar. 2014.
- [25] S. Yi, C. Q. Song, K. Heki, S. C. Kang, Q. Y. Wang, and L. Chang, "Satellite-observed monthly glacier and snow mass changes in Southeast Tibet: Implication for substantial meltwater contribution to the Brahmaputra," *Cryosphere*, vol. 14, no. 7, pp. 2267–2281, Jul. 2020.
- [26] H. Save, S. Bettadpur, and B. D. Tapley, "High-resolution CSR GRACE RL05 mascons," *J. Geophysical Res.-Solid Earth*, vol. 121, no. 10, pp. 7547–7569, Oct. 2016.
- [27] M. M. Watkins, D. N. Wiese, D. N. Yuan, C. Boening, and F. W. Landerer, "Improved methods for observing Earth's time variable mass distribution with GRACE using spherical cap mascons," *J. Geophysical Res.-Solid Earth*, vol. 120, no. 4, pp. 2648–2671, Apr. 2015.
- [28] B. D. Loomis, S. B. Luthcke, and T. J. Sabaka, "Regularization and error characterization of GRACE mascons," *J. Geodesy*, vol. 93, no. 9, pp. 1399–1399, Sep. 2019.
- [29] H. T. Gu et al., "Seasonal catchment memory of high mountain rivers in the Tibetan Plateau," *Nature Commun.*, vol. 14, no. 1, Jun. 2023, Art. no. 3173.
- [30] Y. J. Pan et al., "Interannual variability of vertical land motion over high mountain central Asia from GPS and GRACE/GRACE-FO observations," *GPS Solutions*, vol. 27, no. 4, pp. 1–14, Oct. 2023.
- [31] X. Y. Li et al., "Climate change threatens terrestrial water storage over the Tibetan Plateau," *Nature Climate Change*, vol. 12, no. 9, pp. 801–807, Sep. 2022.
- [32] F. Y. Zhao, D. Long, X. D. Li, Q. Huang, and P. F. Han, "Rapid glacier mass loss in the Southeastern Tibetan Plateau since the year 2000 from satellite observations," *Remote Sens. Environ.*, vol. 270, 2022, Art. no. 112853.
- [33] W. L. Jing, P. Y. Zhang, and X. D. Zhao, "A comparison of different GRACE solutions in terrestrial water storage trend estimation over Tibetan Plateau," *Sci. Rep.*, vol. 9, no. 1, Feb. 2019, Art. no. 1765.
- [34] D. G. Vaughn et al., "Observations: Cryosphere," in *Intergovernmental Panel on Climate Change (Ed.), Climate Change 2013: The Physical Science Basis. Contribution of Working Group I to the Fifth Assessment Report of the Intergovernmental Panel on Climate Change*. Cambridge, UK: Cambridge University Press, pp. 317–382, 2014.
- [35] T. Bolch et al., *Status and Change of the Cryosphere in the Extended Hindu Kush Himalaya Region*. Berlin, Germany: Springer-Verlag, 2019.
- [36] W. T. Pfeffer et al., "The Randolph glacier inventory: A globally complete inventory of glaciers," *J. Glaciology*, vol. 60, no. 221, pp. 537–552, 2014.
- [37] Y. J. Li, F. Li, D. H. Shanguan, and Y. J. Ding, "A new global gridded glacier dataset based on the Randolph glacier inventory version 6.0," *J. Glaciology*, vol. 67, no. 264, pp. 773–776, Aug. 2021.
- [38] C. Qiujie, "Tongji-GRACE2022: New global temporal earth's gravity field models derived from k-band and LRI inter-satellite range-rate data," in *Proc. 28th Gen. Assem. Int. Union Geodesy Geophys.*, 2023.
- [39] S. Swenson, D. Chambers, and J. Wahr, "Estimating geocenter variations from a combination of GRACE and ocean model output," *J. Geophysical Res.-Solid Earth*, vol. 113, no. B8, pp. 1–12, Aug. 2008.
- [40] Y. Sun, R. Riva, and P. Ditmar, "Optimizing estimates of annual variations and trends in geocenter motion and J2 from a combination of GRACE data and geophysical models," *J. Geophys. Res. Solid Earth*, vol. 121, pp. 8352–8370, Nov. 2016.
- [41] B. D. Loomis, K. E. Rachlin, D. N. Wiese, F. W. Landerer, and S. B. Luthcke, "Replacing GRACE/GRACE-FO C<sub>30</sub> with satellite laser ranging: Impacts on Antarctic Ice Sheet mass change," *Geophys. Res. Lett.*, vol. 47, 2020, Art. no. e2019GL085488.
- [42] H. Save, "CSR GRACE and GRACE-FO RL06 mascon solutions v02," 2020, doi: [10.15781/cgq9-nh24](https://doi.org/10.15781/cgq9-nh24).
- [43] X. Li, D. Long, Q. Huang, P. Han, F. Zhao, and Y. Wada, "A high temporal resolution lake data set from multisource altimetric missions and Landsat archives of water level and storage changes on the Tibetan Plateau during 2000–2017 [dataset publication series]," PANGAEA, 2019, doi: <https://doi.org/10.1594/PANGAEA.898411>.
- [44] J. Liao, Y. Zhao, and J. Chen, "A dataset of lake level changes in high mountain Asia using multi-altimeter data," *China Sci. Data*, vol. 5, pp. 1–12, 2019, doi: [10.11922/csdata.2019.0019.zh](https://doi.org/10.11922/csdata.2019.0019.zh).
- [45] H. M. Schmied et al., "The global water resources and use model WaterGAP v2.2d: Model description and evaluation," *Geosci. Model Develop.*, vol. 14, no. 2, pp. 1037–1079, Feb. 2021.
- [46] R. Hugonnet et al., "Accelerated global glacier mass loss in the early twenty-first century," *Nature*, vol. 592, no. 7856, pp. 726–731, Apr. 2021.
- [47] M. Huss, "Density assumptions for converting geodetic glacier volume change to mass change," *Cryosphere*, vol. 7, no. 3, pp. 877–887, 2013.
- [48] O. Baur and N. Sneeuw, "Assessing Greenland ice mass loss by means of point-mass modeling: A viable methodology," *J. Geodesy*, vol. 85, no. 9, pp. 607–615, Sep. 2011.
- [49] P. Ditmar, "Conversion of time-varying Stokes coefficients into mass anomalies at the Earth's surface considering the Earth's oblateness," *J. Geodesy*, vol. 92, no. 12, pp. 1401–1412, Dec. 2018.
- [50] A. Tikhonov, "Solution of incorrectly formulated problems and the regularization method," *Sov. Math.*, vol. 5, pp. 1035–1038, 1963.
- [51] A. E. Hoerl and R. W. Kennard, "Ridge regression: Biased estimation for nonorthogonal problems," *Technometrics*, vol. 42, no. 1, pp. 80–86, Feb. 2000.
- [52] P. L. Xu and R. Rummel, "A simulation study of smoothness methods in recovery of regional gravity fields," *Geophys. J. Int.*, vol. 117, pp. 472–486, 1994, doi: [10.1111/j.1365-246X.1994.tb03945.x](https://doi.org/10.1111/j.1365-246X.1994.tb03945.x).
- [53] W. Wang, Y. Z. Shen, Q. J. Chen, and T. Y. Chen, "One-degree resolution mascon solution over Antarctic derived from GRACE level-2 data," *Front. Earth Sci.*, vol. 11, 2023, Art. no. 1129628.
- [54] W. Wang, Y. Z. Shen, Q. J. Chen, and F. W. Wang, "High-resolution mascon solutions reveal glacier-scale mass changes over the Greenland ice sheet from 2002 to 2022," *Geophysical J. Int.*, vol. 236, no. 1, pp. 494–515, Nov. 2023.
- [55] M. Rodell et al., "The global land data assimilation system," *Bull. Amer. Meteorological Soc.*, vol. 85, no. 3, pp. 381–394, Mar. 2004.
- [56] W. R. Peltier, D. F. Argus, and R. Drummond, "Comment on 'an assessment of the ICE-6G\_C (VM5a) glacial isostatic adjustment model' by Purcell et al.," *J. Geophysical Res.-Solid Earth*, vol. 123, no. 2, pp. 2019–2028, Feb. 2018.
- [57] B. Smith et al., "Pervasive ice sheet mass loss reflects competing ocean and atmosphere processes," *Science*, vol. 368, no. 6496, pp. 1239–1242, Jun. 2020.
- [58] L. Caron, E. R. Ivins, E. Larour, S. Adhikari, J. Nilsson, and G. Blewitt, "GIA model statistics for GRACE hydrology, cryosphere, and ocean science," *Geophysical Res. Lett.*, vol. 45, no. 5, pp. 2203–2212, Mar. 2018.
- [59] H. S. Wang et al., "Load love numbers and green's functions for elastic earth models PREM, iasp91, ak135, and modified models with refined crustal structure from Crust 2.0," *Comput. Geosci.*, vol. 49, pp. 190–199, Dec. 2012.
- [60] F. Brun, E. Berthier, P. Wagnon, A. Käab, and D. Treichler, "A spatially resolved estimate of high mountain Asia glacier mass balances from 2000 to 2016," *Nature Geosci.*, vol. 11, no. 7, pp. 543–543, Jul. 2018.
- [61] D. E. Shean, S. Bhushan, P. Montesano, D. R. Rounce, A. Arendt, and B. Osmanoglu, "A systematic, regional assessment of high mountain Asia glacier mass balance," *Front. Earth Sci.*, vol. 7, pp. 1–19, Jan. 2020.
- [62] A. S. Gardner, "A reconciled estimate of glacier contributions to sea level rise: 2003 to 2009," *Science*, vol. 340, no. 6137, pp. 1168–1168, Jun. 2013.
- [63] D. Farinotti, W. W. Immerzeel, R. J. de Kok, D. J. Quincey, and A. Dehecq, "Manifestations and mechanisms of the Karakoram glacier Anomaly," *Nature Geosci.*, vol. 13, no. 1, pp. 8–16, Jan. 2020.
- [64] N. Forsythe, H. J. Fowler, X. F. Li, S. Blenkinsop, and D. Pritchard, "Karakoram temperature and glacial melt driven by regional atmospheric circulation variability," *Nature Climate Change*, vol. 7, no. 9, pp. 664–670, Sep. 2017.
- [65] Q. Y. Wang and W. K. Sun, "Seasonal cycles of high mountain Asia glacier surface elevation detected by ICESat-2," *J. Geophysical Res.-Atmos.*, vol. 127, no. 23, Dec. 2022, Art. no. e2022JD037501.



- [66] T. D. Yao et al., "Different glacier status with atmospheric circulations in Tibetan Plateau and surroundings," *Nature Climate Change*, vol. 2, no. 9, pp. 663–667, Sep. 2012.
- [67] L. Jakob, N. Gourmelen, M. Ewart, and S. Plummer, "Spatially and temporally resolved ice loss in high mountain Asia and the Gulf of Alaska observed by CryoSat-2 swath altimetry between 2010 and 2019," *Cryosphere*, vol. 15, no. 4, pp. 1845–1862, Apr. 2021.
- [68] Y. B. Fan, C. Q. Ke, X. B. Zhou, X. Y. Shen, X. N. Yu, and D. Lhakpa, "Glacier mass-balance estimates over high mountain Asia from 2000 to 2021 based on ICESat-2 and NASADEM," *J. Glaciology*, vol. 69, no. 275, pp. 500–512, Jun. 2023.
- [69] Q. Y. Wang, S. Yi, and W. K. Sun, "Continuous estimates of glacier mass balance in high mountain Asia based on ICESat-1,2 and GRACE/GRACE follow-on data," *Geophysical Res. Lett.*, vol. 48, no. 2, Jan. 2021, Art. no. e2020GL090954.
- [70] M. Zemp et al., "Global glacier mass changes and their contributions to sea-level rise from 1961 to 2016," *Nature*, vol. 577, no. 7792, pp. E9–E9, Jan. 2020.
- [71] A. Kääb, D. Treichler, C. Nuth, and E. Berthier, "Brief communication: Contending estimates of 2003-2008 glacier mass balance over the Pamir-Karakoram-Himalaya," *Cryosphere*, vol. 9, no. 2, pp. 557–564, 2015.
- [72] D. Treichler, A. Kääb, N. Salzmann, and C. Y. Xu, "Recent glacier and lake changes in high mountain Asia and their relation to precipitation changes," *Cryosphere*, vol. 13, no. 11, pp. 2977–3005, Nov. 2019.
- [73] D. Farinotti et al., "Substantial glacier mass loss in the Tien Shan over the past 50 years," *Nature Geosci.*, vol. 8, no. 9, pp. 716–722, Sep. 2015.
- [74] A. Bhattacharya et al., "High mountain Asian glacier response to climate revealed by multi-temporal satellite observations since the 1960s," *Nature Commun.*, vol. 12, no. 1, Jul. 2021, Art. no. 4133.



**Wei Wang** received the B.S. degree in surveying and geoinformatics from the Shandong University of Science and Technology, Qingdao, China, in 2019. She is currently working toward the Ph.D. degree in survey and mapping with the College of Surveying and Geo-Informatics, Tongji University, Shanghai, China.

Her research interests include mascon modeling from time-variable gravity model and its application in cryosphere and hydrology.



**Yunzhong Shen** received the Ph.D. degree in geophysical geodesy from the Institute of Geodesy and Geophysics, Chinese Academy of Sciences, Beijing, China, in 2000.

He is currently a Professor with the College of Surveying and Geo-informatics, Tongji University, Shanghai, China. His main research includes the regularized solution to the ill-conditioned inverse problem of recovering a gravitational potential model from satellite-to-satellite tracking data, as well as variance component and parameter estimation theory. His research interests include geodetic data processing on satellite gravimetry and satellite positioning.

Dr. Shen is an Editor of *Journal of Geodesy* and *Acta Geodetica et Cartographica Sinica*.



**Qiujiu Chen** received the B.S. degree in surveying and mapping engineering from the Guangdong University of Technology, Guangzhou, Guangdong, China, in 2007, and the Ph.D. degree in geodesy from the Tongji University, Shanghai, China, in 2016.

He is currently a Professor with the College of Surveying and Geo-Informatics, Tongji University. His research interests include short-arc approach for satellite-based gravity field determination, frequency-dependent noise modeling, non-gravitational acceleration calibration, regularization methodologies, mascon modeling, and simulations for next-generation gravity satellites.



**Fengwei Wang** received the B.S. degree in surveying and geoinformatics from the Shandong University of Science and Technology, Qingdao, China, in 2011, and the Ph.D. degree in geodesy from the Tongji University, Shanghai, China, in 2021.

He is currently a Postdoctoral researcher with the State Key Laboratory of Marine Geology, Tongji University. His research interests include satellite gravity, ocean mass change, and multichannel singular spectrum analysis.